

How a small noise generates large-amplitude oscillations of volcanic plug and provides high seismicity

Dmitri V. Alexandrov^a, Irina A. Bashkirtseva, and Lev B. Ryashko

Department of Mathematical Physics, Ural Federal University, Lenina ave., 51, 620000 Ekaterinburg, Russia

Received 20 February 2015 / Received in final form 25 March 2015

Published online 20 April 2015 – © EDP Sciences, Società Italiana di Fisica, Springer-Verlag 2015

Abstract. A non-linear behavior of dynamic model of the magma-plug system under the action of N -shaped friction force and stochastic disturbances is studied. It is shown that the deterministic dynamics essentially depends on the mutual arrangement of an equilibrium point and the friction force branches. Variations of this arrangement imply bifurcations, birth and disappearance of stable limit cycles, changes of the stability of equilibria, system transformations between mono- and bistable regimes. A slope of the right increasing branch of the friction function is responsible for the formation of such regimes. In a bistable zone, the noise generates transitions between small and large amplitude stochastic oscillations. In a monostable zone with single stable equilibrium, a new dynamic phenomenon of noise-induced generation of large amplitude stochastic oscillations in the plug rate and pressure is revealed. A beat-type dynamics of the plug displacement under the influence of stochastic forcing is studied as well.

1 Introduction

It has long been known that the dynamics of volcanic systems is very complex due to different non-linear processes leading to a great variety of possible states during the same eruption [1,2]. The most critical questions when, where and how volcanic eruptions happen will remain to a great extent empirical without modeling predictions of their non-linear dynamics. Therefore, formulation and development of suitable mathematical models of volcanic behavior represents an important research problem [3–6].

A great number of uncertainties in geophysical and chemical parameters of volcanic eruptions [7] testifies that volcanoes (similar to many climate systems modeled in terms of probabilities [8–10]) represent stochastic and chaotic systems [11,12]. An important point is that some interactions between system nonlinearities and noises therewith are responsible for the origination and evolution of different probabilistic effects. So, among others, noise-induced transitions [13], noise-induced chaos [14,15], stochastic resonance [16,17] and multiresonance [18] may be mentioned. It is important to keep in mind that stochastic phenomena frequently met in a lot of non-linear models are the subjects of active studies in different research areas [13,19–24].

An important point is that a variety of silicic volcanoes closely studied during the last decades demonstrate an intricate oscillatory behavior [25–28]. So, for example, the Mount St. Helen's dome-building eruption in 2004 and

2005 has demonstrated a near-equilibrium cyclic behavior, during which the solid plug uplift was caused by magma flux from below with a practically steady-state rate of the order $1\text{--}2\text{ m}^3\text{ s}^{-1}$. This volcanic eruption was accompanied by repetitive drumbeat earthquakes of a 1–2 min periodicity with focal depth $<1\text{ km}$ and magnitudes <2 [29–31]. A nearly periodic behavior of such drumbeat seismicity can be explained by stick-slip motions of a volcanic plug [25,28]. A new nonlinear dynamic model of the plug motion based on this stick-slip mechanism was suggested in reference [29]. This model connects the plug dynamics with a damped oscillator. Below we use this differential model to demonstrate unusual nonlinear dynamics of plug motions and, in particular, origination of the large amplitude stochastic oscillations (LASO) even in the presence of small noises.

A new evolutionary model describing non-linear plug dynamics based on experimental data of the Mount St. Helen's (MSH) eruption was derived and discussed in detail in reference [29]. A scheme of this process representing recurrent stick-slip dynamics of the solid plug along its margins with the friction force F is illustrated in Figure 1.

Let us pay our attention to the main physical aspects of this process. The magma flux inflows into the base of an eruptive conduit with practically steady-state rate Q . A dacite plug of solidified magma therewith clogs the upper part of conduit. In addition, the solid plug is mobile because of basal accretion with mass rate ρB and pressure p acting from below (here ρ and B being the magma bulk density and the volumetric rate of magma solidification). The plug mass m is dependent of time t as $m = m_0 + \kappa t$

^a e-mail: Dmitri.Alexandrov@usu.ru

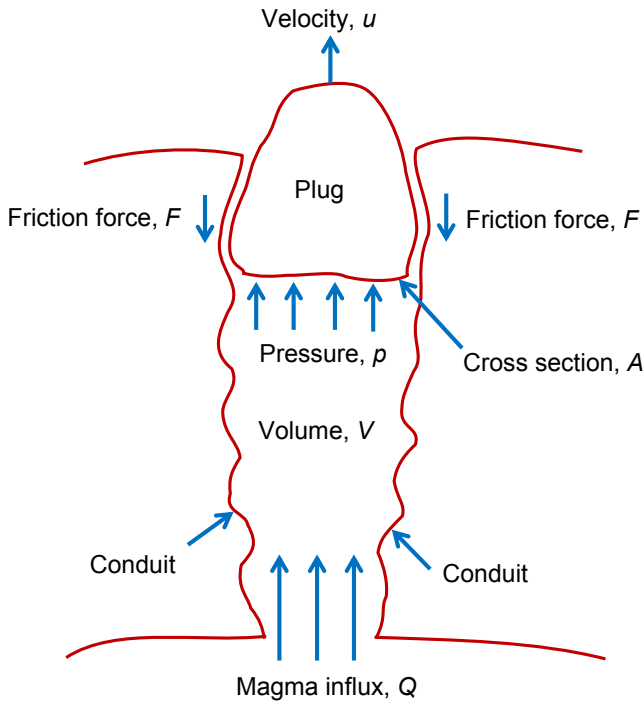


Fig. 1. A scheme of the plug dynamics after Iverson et al. [29].

due to the difference in mass rates ρB and $\rho_r E$ (here m_0 is the initial plug mass, ρ_r is the bulk density of plug, E is the volumetric rate of surface erosion, and $\kappa = \rho B - \rho_r E$ is assumed constant). Since the solidification of magma and erosion are both too slow to induce changes of the plug mass with time, in the present paper, the plug mass is assumed to be constant $\kappa = 0$. Other physical parameters such as the magma compressibility α_1 , the conduit wall compliance α_2 and the horizontal cross-sectional area A , are estimated by Iverson et al. [29].

An important point of the model is that a non-linear plug dynamics is governed by the friction force F dependent of the plug velocity u and the plug weight mg (here g is the acceleration due to gravity) while the conduit volume V is controlled by the mass conservation. A non-linear differential model of this process containing three independent variables u (plug velocity), p (pressure) and V (conduit volume) was derived by Iverson et al. [29]. We use their model below to demonstrate new stochastically induced effects and dynamic regimes of volcanic plugs.

2 Deterministic model. Attractors and bifurcations

The mathematical model of reduced non-linear equations, which is based on conservation of the solid plug linear momentum, solid plug mass and conduit fluid mass has

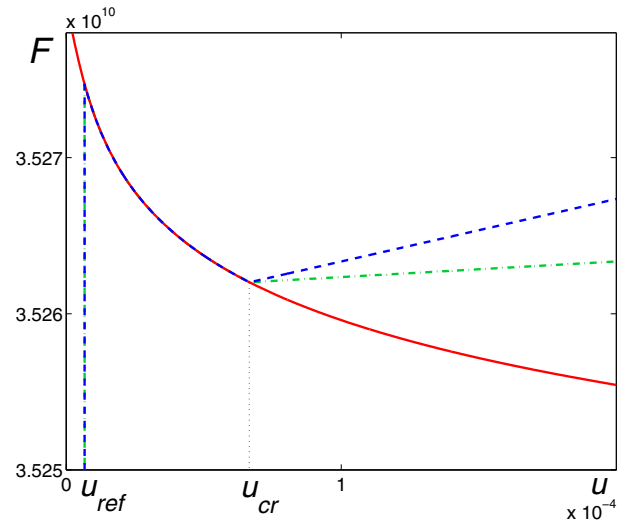


Fig. 2. Plots of the friction functions. The solid line (red online) represents the function $F_0(u)$ (see Eq. (2)). The function $F_N(u)$ is plotted accordingly to expression (3) with $u_{ref} = 6.67 \times 10^{-6} \text{ m s}^{-1}$, $u_{cr} = 10u_{ref}$ for $k_N = 1 \times 10^{10} \text{ kg s}^{-1}$ by the dash-dotted line (green online), and for $k_N = 4 \times 10^{10} \text{ kg s}^{-1}$ by the dashed line (blue online).

the form [29]

$$\begin{aligned} \frac{du}{dt} &= -g + \frac{1}{m_0} (pA - F), \\ \frac{dp}{dt} &= -\frac{1}{(\alpha_1 + \alpha_2)V} (Au + RB - Q), \\ \frac{dV}{dt} &= \frac{\alpha_1}{\alpha_1 + \alpha_2} (Au + RB - Q) + Q - B, \end{aligned} \quad (1)$$

where $R = 1 - \rho/\rho_r = 1 - (\rho_0/\rho_r) \exp[\alpha_1(p - p_0)]$ is found from the isothermal equation of state. Here, p_0 is a static equilibrium pressure, and ρ_0 is a magma density. Physical parameters of this system are [29]: $B = Q = 2 \text{ m}^3 \text{ s}^{-1}$, $m_0 = 3.6 \times 10^{10} \text{ kg}$, $A = 30000 \text{ m}^2$, $p_0 = 1.2936 \times 10^7 \text{ Pa}$, $\alpha_1 = 10^{-7} \text{ Pa}^{-1}$, $\alpha_2 = 10^{-9} \text{ Pa}^{-1}$, $F_0 = 3.528 \times 10^{10} \text{ kg m s}^{-2}$, $u_{ref} = 0.1Q/A = 6.67 \times 10^{-6} \text{ m s}^{-1}$, $V_0 = 6.32 \times 10^5 \text{ m}^3$, $c = 1.7 \times 10^{-4}$, $g = 9.8 \text{ m s}^{-2}$, $\rho_0 = \rho_r = 2000 \text{ kg m}^{-3}$.

The main aspects of MSH friction force measured in experiments [30] can be described by a function [29]

$$F = \text{sgn}(u)F_0(u), \quad F_0(u) = F_0 (1 - c \sinh^{-1}|u/u_{ref}|), \quad (2)$$

where $\text{sgn}(u)$ is the sign of u , F_0 is the friction force at static equilibrium, $c \ll 1$ is a rate-weakening parameter and u_{ref} is a reference value of u . Expression (2) describes the main physical features of the plug dynamics: the friction force at $u = 0$ abruptly changes its sign because the gravity force (which shifts the plug in downward direction) is oppositely directed to the friction force. The function $F_0(u)$ is plotted in Figure 2 by the solid (red online) curve.

However, a monotonically decreasing behavior of the friction force (2) is not a good physical approximation of the real friction force for any $u > 0$. It is well-known

that the friction force in complex liquids, suspensions, and flows of magma (see, among others, [28]), is not monotonic and combines decreasing and increasing parts. Usually, for complex nonlinear flows, the friction force has a so-called N -shaped form: for small u , friction $F(u)$ monotonically increases, after that there is a part with negative slope, and further, for sufficiently large u , the function $F(u)$ increases again.

Taking this into account let us model this force by the following close continuous N -shaped function

$$F(u) = \text{sgn}(u)F_N(u), \quad (3)$$

where

$$F_N(u) = \begin{cases} F_0 \frac{u}{u_{\text{ref}}}, & 0 < u < u_{\text{ref}} \\ F_0(u), & u_{\text{ref}} \leq u \leq u_{cr} \\ F_0(u_{cr}) + k_N(u - u_{cr}), & u > u_{cr}. \end{cases}$$

This function sharply increases within the short initial interval $0 < u < u_{\text{ref}}$. In the middle zone, $u_{\text{ref}} \leq u \leq u_{cr}$, the function $F(u) = F_0(u)$ slowly decreases. For $u > u_{cr}$, the function $F(u)$ increases again with positive slope defined by the parameter k_N . Some exemplary plots of the function $F_N(u)$ for $u_{cr} = 10u_{\text{ref}}$ and different k_N are shown in Figure 2 by broken lines.

This N -shaped function $F_N(u)$ generates different dynamic regimes depending on a position of the point u_{cr} where the friction force slope changes its sign. A type of deterministic dynamics depends on the answer to the question: whether on the right or left side of the critical point u_{cr} , the equilibrium point (the point of intersection of nullclines $\dot{u} = 0$, $\dot{p} = 0$) is localized? Namely, if the equilibrium point lies on the decreasing interval (on the left side of u_{cr}), this equilibrium is unstable. In this case, a limit cycle may appear around such unstable equilibrium.

From the other hand, if the equilibrium point lies on the increasing interval (on the right side of u_{cr}), this point is stable. If this is really the case, the dynamic system is locally stable for small deviations from the equilibrium point. However, if deviations from this point are large enough, the system can change its state and, due to its nonlinearity, turn into a stable limit cycle. In this case, the system is bistable. Figure 3 shows possible locations of nullclines so that the lower corner of the friction curve may be placed as follows: (i) on the right side of the pressure nullcline (e.g., $u_{cr} = 11u_{\text{ref}}$), (ii) on the pressure nullcline ($u_{cr} = 10u_{\text{ref}}$) and (iii) on the left side of the pressure nullcline (e.g., $u_{cr} = 9u_{\text{ref}}$).

Let us briefly discuss the system dynamics corresponding to these locations. In case (i), there is an unstable equilibrium with a rather large stable cycle around it. This case was studied in detail in reference [32]. The critical case (ii) demonstrates the same dynamics as case (i). Its numerical modeling however is connected with some difficulties due to the stiff dynamic behavior. The system has a stable equilibrium in case (iii). In what follows, we focus on the case (iii) with fixed $u_{cr} = 9u_{\text{ref}}$ and varying k_N .

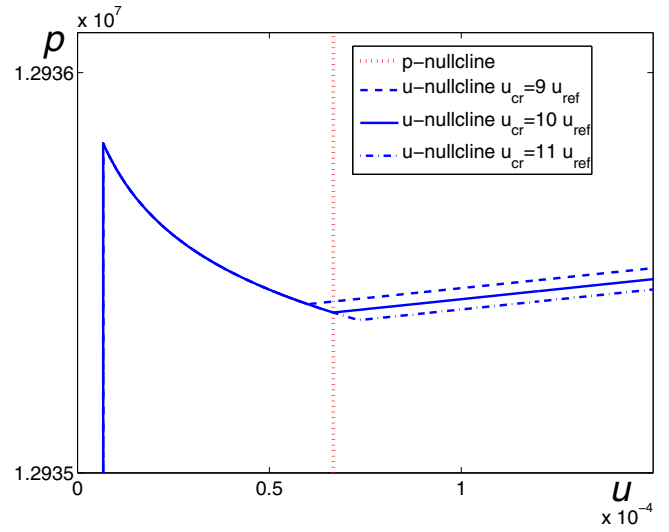


Fig. 3. Nullclines of pressure p (dotted, red online) and velocity u (blue online) for different possible locations of a critical point $u = u_{cr}$: $u_{cr} = 9u_{\text{ref}}$ (dashed), $u_{cr} = 10u_{\text{ref}}$ (solid), and $u_{cr} = 11u_{\text{ref}}$ (dash-dotted).

If k_N is small enough, the equilibrium point is rounded by a big stable cycle (the phase portrait for $k_N = 3 \times 10^{10} \text{ kg s}^{-1}$ is shown in Fig. 4a). Two attractors (the stable equilibrium and the limit cycle) are divided by an unstable cycle. A saddle-node bifurcation (vanishing of a stable cycle) occurs with increasing k_N at a critical value $k_N = k_N^* = 3.37 \times 10^{10} \text{ kg s}^{-1}$. The phase portrait for $k_N = 4 \times 10^{10} \text{ kg s}^{-1} > k_N^*$ is presented in Figure 4b. An important point is that when the stable (blue) and unstable (red) cycles merge together (see Fig. 4a) they vanish and one stable equilibrium (black point) remains only. Some details of such variations in deterministic dynamics of the model are shown in Figure 5.

In Figure 5a, the real parts of eigenvalues of the Jacobi matrix for the equilibrium point are plotted. As one can see, real parts are negative, so this equilibrium is stable for a wide range of the parameter k_N .

In Figure 5b, a bifurcation diagram of this model is presented. Here, u -coordinates of extreme points of attractors and repellers as functions of k_N are shown: stable cycles (thick solid, blue), unstable cycles (thick dashed, red), and stable equilibria (thin black). The unstable cycle separates basins of attraction of the stable cycle and equilibrium. When k_N is small enough, the unstable cycle is very close to equilibrium, and a basin of equilibrium attraction is quite small. With increasing k_N , this increasing unstable cycle moves away from the equilibrium and approaches the stable cycle. At the bifurcation point k_N^* , they merge and annihilate. For $k_N > k_N^*$, a stable equilibrium is a single attractor of the system.

In what follows, a mutual arrangement of the equilibrium and both cycles is essential for the understanding of probabilistic mechanisms of the generation of large and small amplitude stochastic oscillations (LASO and SASO, respectively).

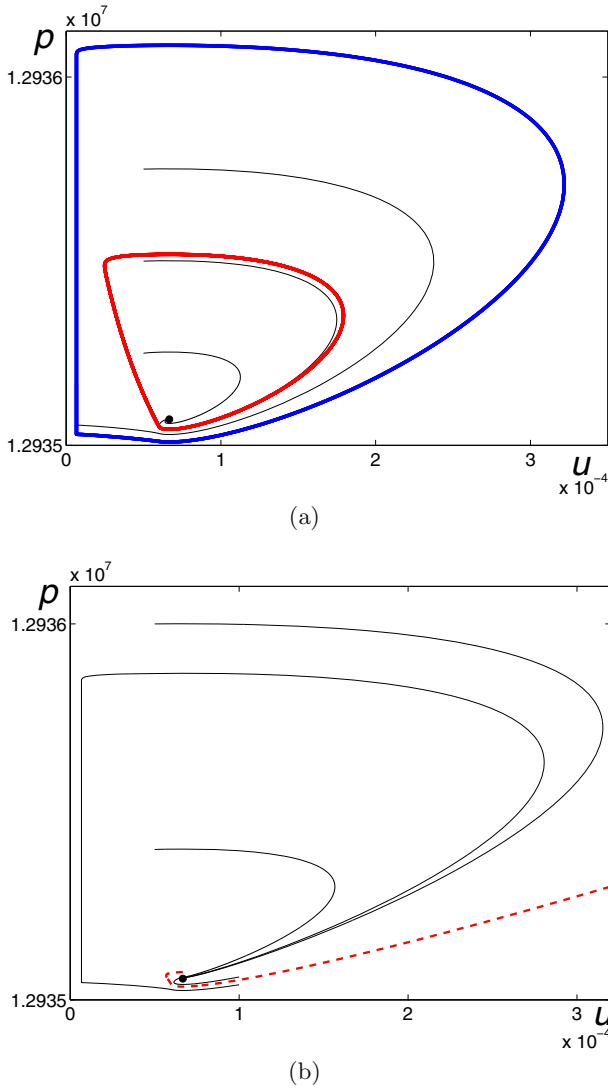


Fig. 4. Phase portraits for $u_{cr} = 9u_{ref}$ at $k_N = 3 \times 10^{10} \text{ kg s}^{-1}$ (a) and $k_N = 4 \times 10^{10} \text{ kg s}^{-1}$ (b). The thick lines mark cycles: stable (external, blue online) and unstable (internal, red online) ones (upper panel). The black points show the stable equilibria. The pseudo-separatrix is plotted by the dashed line (lower panel).

3 Stochastic dynamics

In order to study the role of random noise on system dynamics let us replace the first deterministic equation in equation (1) by the following stochastic equation (in Ito sense) [33]

$$\frac{du}{dt} = -g + \frac{1}{m_0} (pA - F(u)) - \frac{\varepsilon F(u)\xi(t)}{m_0}, \quad (4)$$

where $\xi(t)$ is a standard Gaussian white noise with parameters $\langle \xi(t) \rangle = 0$, $\langle \xi(t)\xi(\tau) \rangle = \delta(t - \tau)$, and ε is the intensity of multiplicative noise modelling random disturbances in the friction force. The stochastic model (4) is obtained from the deterministic model (1) after replacing: $F(u) \rightarrow F(u)(1 + \varepsilon\xi)$.

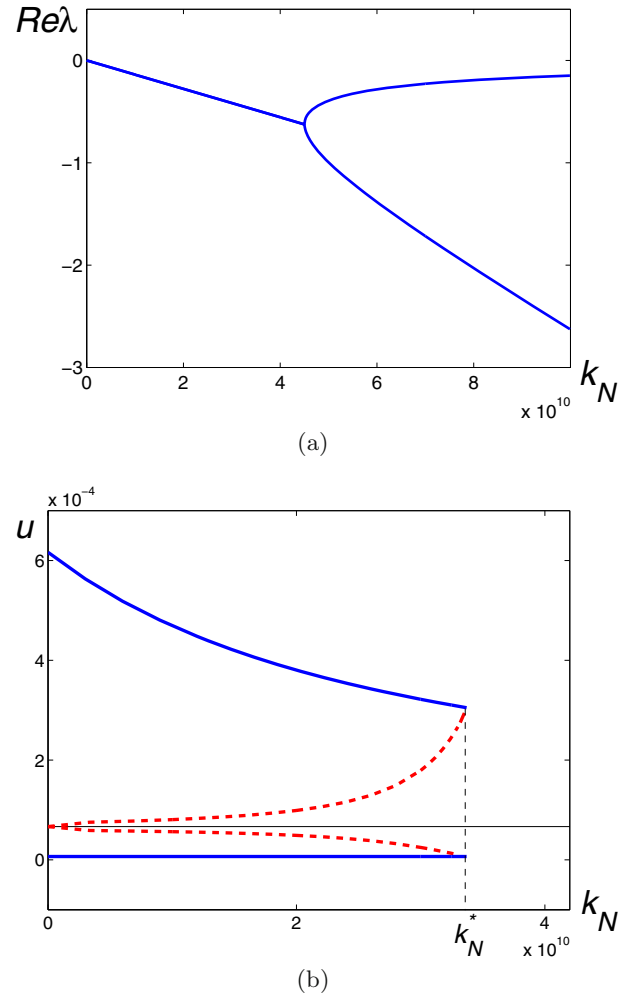


Fig. 5. Characteristics of the deterministic system. (a) Real parts of eigenvalues of the Jacobi matrix for equilibrium, (b) u -coordinates of extreme points of attractors and repellers as functions of k_N for $u_{cr} = 9u_{ref}$: stable cycles (thick solid, blue online), unstable cycles (thick dashed, red online), and equilibria (thin line). The value k_N^* marks the saddle-node bifurcation point.

Here, we fix $u_{cr} = 9u_{ref}$ and study a stochastic behavior for different k_N determining the slope of the friction force (3).

In numerical simulation of random trajectories, we used the Euler-Maruyama method [34] with time step 10^{-5} s. To generate the independent, standard, and normally distributed pseudo-random numbers modeling stochastic disturbances, we applied the Box-Muller transform [35].

Let $k_N = 3 \times 10^{10} \text{ kg s}^{-1}$ (see Fig. 4 for the deterministic model). In this case, a stable equilibrium and a stable cycle coexist in the deterministic system. Also let this equilibrium point represents the initial state. Then stochastic trajectories lie in the vicinity of the equilibrium point for small noise ($\varepsilon = 4 \times 10^{-6}$) and the system has a SASO-type dynamics (a small spot in Fig. 6a, grey color online). With increasing the noise intensity,

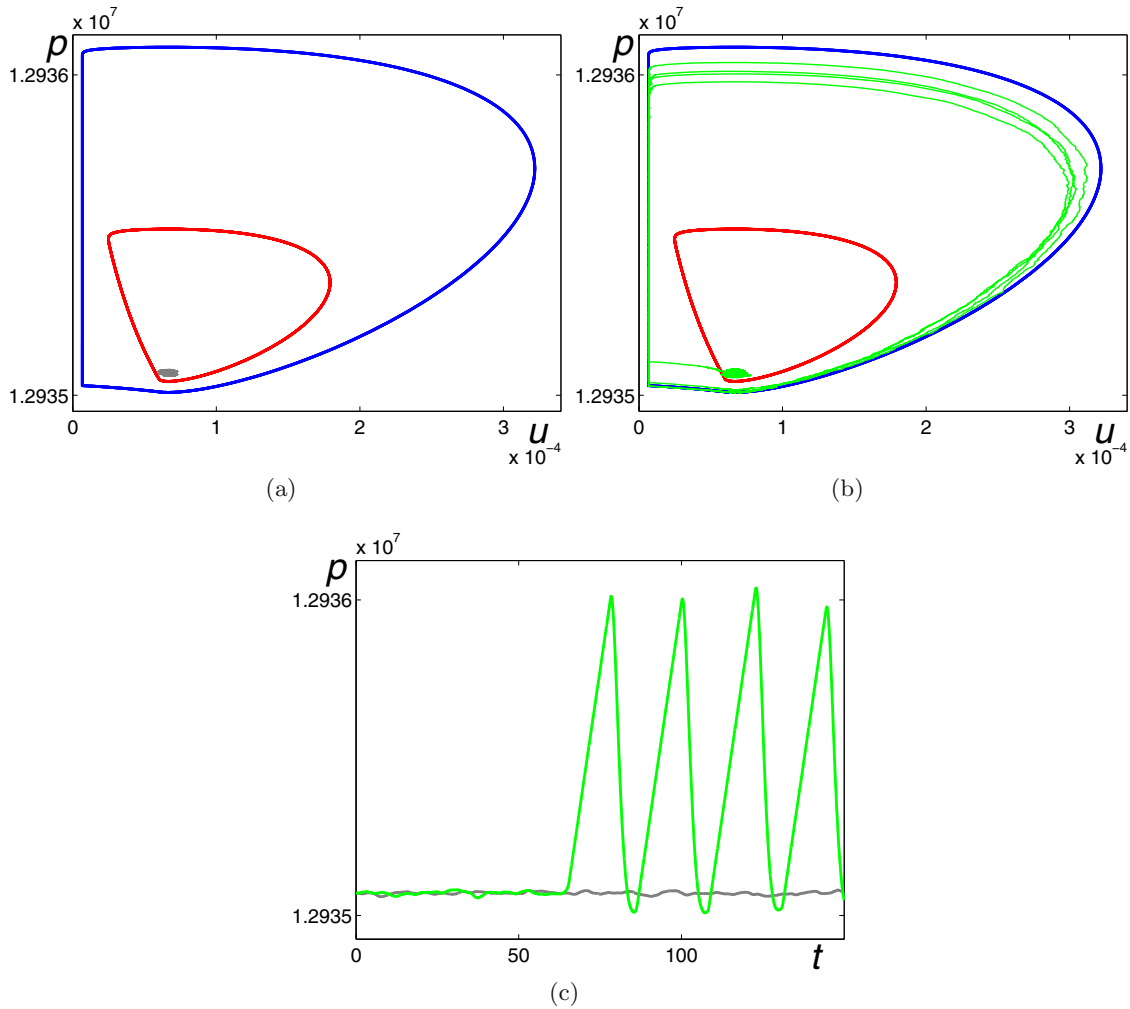


Fig. 6. Stochastic phase trajectories for $u_{cr} = 9u_{ref}$, $k_N = 3 \times 10^{10} \text{ kg s}^{-1}$: (a) $\varepsilon = 3 \times 10^{-6}$ (grey online), (b) $\varepsilon = 4 \times 10^{-6}$ (green online), (c) time series.

stochastic trajectories leave the basin of attraction of this equilibrium point, cross the separatrix (red line) and are attracted to the stable cycle (blue line) (see Fig. 6b, green color). Thus, a noise-induced transition from SASO to LASO takes place. The time series demonstrating this transition are presented in Figure 6c. An important point is that the plug velocity increases abruptly by action of stochastic noises.

A very important phenomenon of generation of noise-induced oscillations occurs with increasing the noise intensity in the region where the deterministic system exhibits just a stable equilibrium. So, for example, if $k_N = 4 \times 10^{10} \text{ kg s}^{-1}$, the deterministic system has a single attractor – a point of stable equilibrium. As would be expected, stochastic trajectories are localized near this equilibrium point in the case of small noises ($\varepsilon = 3 \times 10^{-6}$). This SASO-type dynamics is shown in Figure 7 by the grey color.

As noise intensity increases ($\varepsilon = 10 \times 10^{-6}$), stochastic trajectories going away from the equilibrium point generate the LASO-type dynamics (green color in Fig. 7). Note

that in the framework of deterministic model, such large amplitude oscillations are impossible.

An underlying reason of this noise-induced phenomenon is connected with peculiarities of the phase portrait of the deterministic system. Indeed, small deviations from the equilibrium result in small-amplitude trajectories that correspond to the subthreshold response. If we take initial deviations larger than some threshold, large-amplitude trajectories with “long excursions” appear (see Figs. 4b and 7c). This corresponds to the suprathreshold response. Around the equilibrium, one can find a set of initial points corresponding to the subthreshold response. This subthreshold domain is detached from the suprathreshold motion by the curve called “pseudo-separatrix”. In Figures 4b and 7c, this pseudo-separatrix is plotted by the dashed red lines. For weak noise ($\varepsilon = 3 \times 10^{-6}$), random trajectories of the stochastic system starting from equilibrium do not cross this pseudo-separatrix and localize in the subthreshold domain. For increasing noise ($\varepsilon = 10 \times 10^{-6}$), the trajectories with high probability can cross the pseudo-separatrix and continue to move

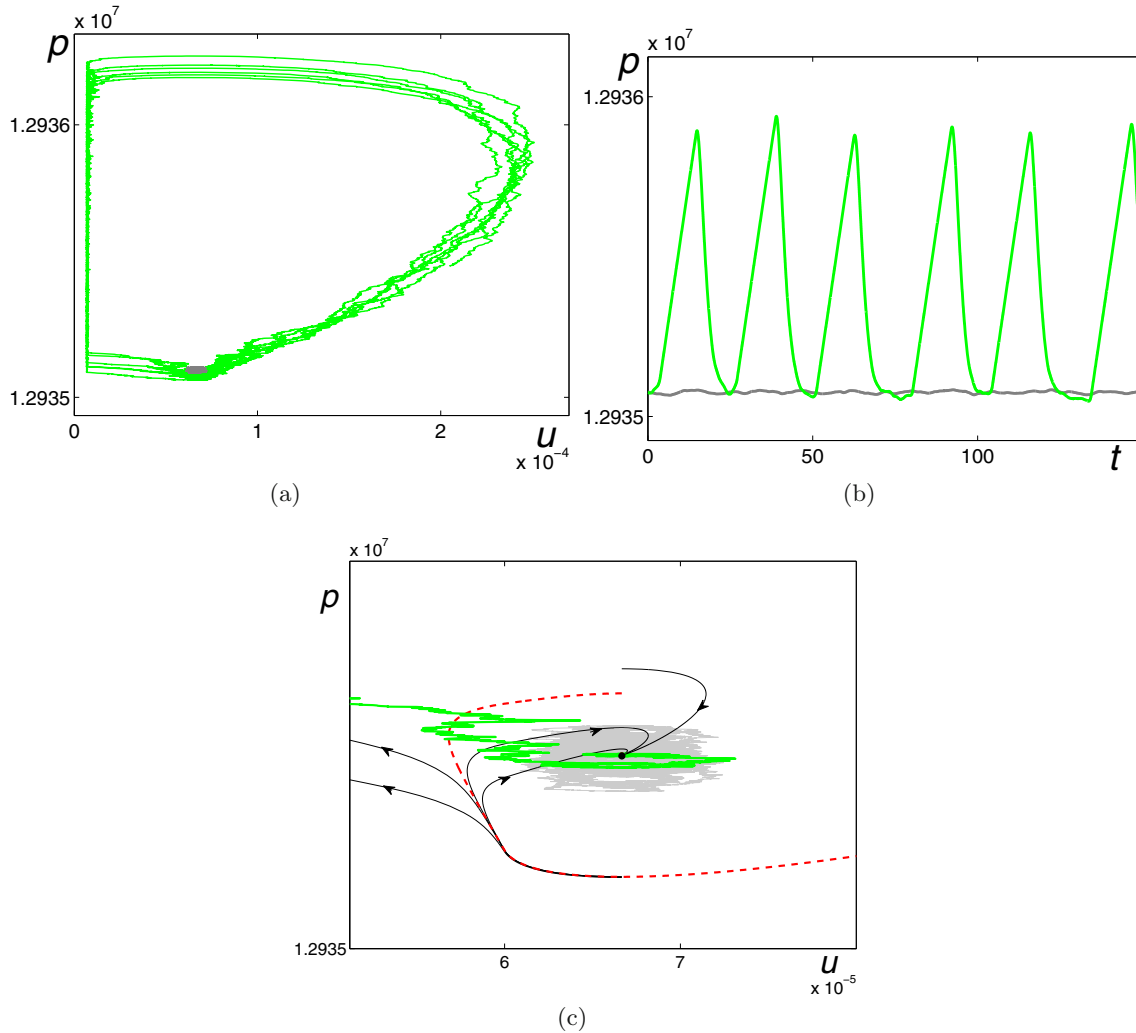


Fig. 7. Stochastic phase trajectories for $u_{cr} = 9u_{ref}$, $k_N = 4 \times 10^{10} \text{ kg s}^{-1}$: (a) $\varepsilon = 3 \times 10^{-6}$ (grey online) and $\varepsilon = 10 \times 10^{-6}$ (green online); (b) time series; (c) an enlarged fragment with pseudoseparatrix (red online).

in the suprathreshold zone far from the equilibrium (see Fig. 7).

Thus, a new dynamic scenario of noise-induced generation of large-amplitude stochastic oscillations appears with increasing the noise intensity.

Consider now how the transition from SASO to LASO dynamics affects the plug displacement $d(t) = \int_0^t u(\tau) d\tau$. Some changes in dynamics of plug displacement are shown in Figure 8. For weak noise $\varepsilon = 3 \times 10^{-6}$, a motion of plug is close to uniform. An increase of noise intensity up to $\varepsilon = 10 \times 10^{-6}$ breaks up this uniformity and leads to a drumbeat-type beats of the plug displacement. As one can see, abrupt changes in the volcanic activity occur with an unessential increase of noise intensity.

4 Conclusion

The presence of a N -shaped form of the friction force in deterministic model leads to the variability in dynamics.

The system can exhibit the monostable (just equilibrium or cycle) and bistable (both of them) regimes. We studied a dynamics near the saddle-node bifurcation where the system demonstrates a phenomenon of abrupt vanishing of self-oscillations. Namely, the dynamic system under consideration possesses a single stable point of equilibrium instead of a cycle. At first glance it would seem that the magma flux under the plug is stabilizing and going to a constant value. However, the stochastic analysis demonstrates that this is not the case. So, for instance, even sufficiently small external noises cause some stochastic large amplitude oscillations of the main physical parameters (plug velocity and pressure) in regions with a single stable equilibrium point due to high excitability of the dynamic system. It is worth noting that the non-linear volcano model under consideration is a new significant example of an expanding collection [19] of excitable systems attracting an increasing interest of researchers.

In the present paper, an important point is that whether the contribution of large amplitude oscillations

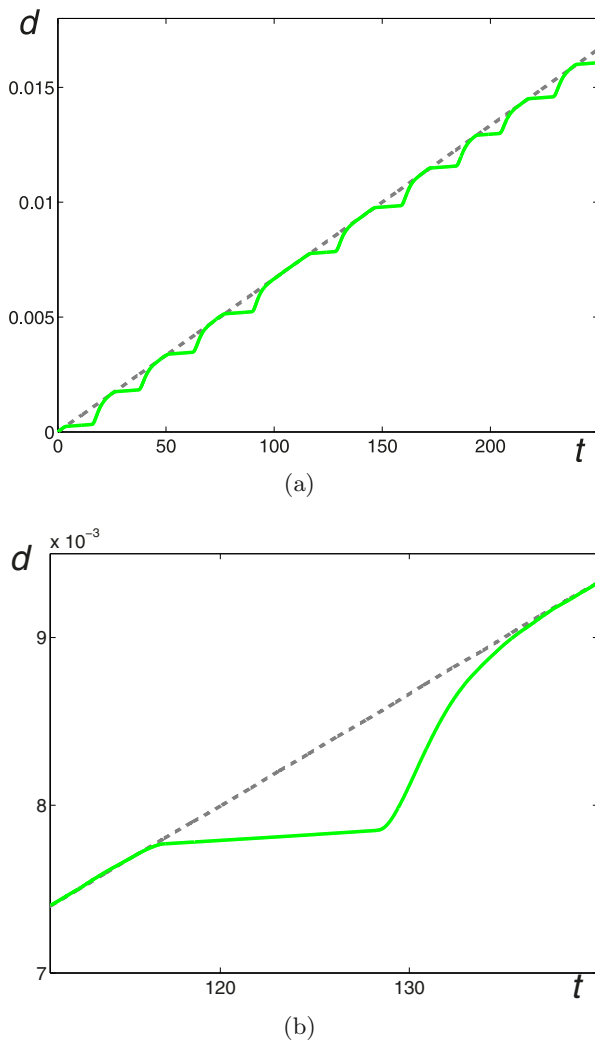


Fig. 8. (a) Displacement d (measured in meters) as a function of time t (measured in seconds) for $u_{cr} = 9u_{ref}$, $k_N = 4 \times 10^{10} \text{ kg s}^{-1}$, $\varepsilon = 3 \times 10^{-6}$ (dashed, grey online) and $\varepsilon = 10 \times 10^{-6}$ (solid, green online); (b) an enlarged fragment.

(LASO) or small amplitude oscillations (SASO) is dominated in a non-linear behavior. So, if the slope coefficient k_N of the right branch of the friction function is small enough (when the unstable cycle shown by the red dashed lines in Fig. 5b merges with the equilibrium point shown by the black solid line), the non-linear system demonstrates a LASO-type dynamics. The stable and unstable cycles merge together (so that the ends of the red dashed and blue solid lines come together) with increasing k_N . In this case, the SASO regime is dominated. On further increasing of k_N the dynamic system has a point of equilibrium (just the black solid line) with a rather large basin of attraction (Fig. 5b).

A noise-induced transformation from SASO to LASO-type regime significantly changes the dynamics of plug displacement. It is of prime importance that an increase of noise intensity leads to a drumbeat-type beats of the plug displacement with irregular periodicity dependent of noise. In addition, the periods of monotonic growth are

replaced by the periods of nearly constant displacement, which in their turn, are changed by the time intervals with abrupt increasing of the plug displacement. Such a beat-type behavior is a building block for understanding the physical mechanisms of volcanic drumbeat seismicity.

This work was supported by the Ministry of Education and Science of the Russian Federation under the project No. 315.

References

1. R.G. Vaughan, S.J. Hook, M.S. Ramsey, V.J. Realmuto, D.J. Schneider, *Geophys. Res. Lett.* **32**, L19305 (2005)
2. H.K.M. Tanaka, T. Kusagaya, H. Shinohara, *Nat. Commun.* **5**, 3381 (2014)
3. O.E. Melnik, R.S.J. Sparks, *Nature* **402**, 37 (1999)
4. A. Barmin, O. Melnik, R.S.J. Sparks, *Earth Planet. Sci. Lett.* **199**, 173 (2002)
5. M. Nakanishi, T. Koyaguchi, *J. Volcanol. Geother. Res.* **178**, 46 (2008)
6. A. Costa, G. Wadge, O. Melnik, *Earth Planet. Sci. Lett.* **337-338**, 39 (2012)
7. G. Woo, *The Mathematics of Natural Catastrophes* (Imperial College Press, 2000)
8. B. Saltzman, *Dynamical Paleoclimatology: Generalised Theory of Global Climate Change* (Academic Press, San Diego, 2002)
9. D.V. Alexandrov, I.A. Bashkirtseva, L.B. Ryashko, *Tellus A* **66**, 23454 (2014)
10. D.V. Alexandrov, I.A. Bashkirtseva, S.P. Fedotov, L.B. Ryashko, *Eur. Phys. J. B* **87**, 227 (2014)
11. R.S.J. Sparks, *Earth Planet. Sci. Lett.* **210**, 1 (2003)
12. M.S. Bebbington, W. Marzocchi, *J. Geophys. Res.* **116**, B05204 (2011)
13. W. Horstemke, R. Lefever, *Noise-Induced Transitions* (Springer, Berlin, 1984)
14. Y.C. Lai, T. Tél, *Transient Chaos: Complex Dynamics on Finite Time Scales* (Springer, Berlin, 2011)
15. I. Bashkirtseva, G. Chen, L. Ryashko, *Chaos* **22**, 033104 (2012)
16. L. Gammaitoni, P. Hänggi, P. Jung, F. Marchesoni, *Rev. Mod. Phys.* **70**, 223 (1998)
17. M.D. McDonnell, N.G. Stocks, C.E.M. Pearce, D. Abbott, *Stochastic Resonance: from Suprathreshold Stochastic Resonance to Stochastic Signal Quantization* (Cambridge University Press, Cambridge, 2008)
18. J.J. Torres, J. Marro, J.F. Mejias, *New J. Phys.* **13**, 053014 (2011)
19. B. Lindner, J. Garcia-Ojalvo, A. Neiman, L. Schimansky-Geier, *Phys. Rep.* **392**, 321 (2004)
20. P. Hänggi, F. Marchesoni, *Rev. Mod. Phys.* **81**, 387 (2009)
21. I. Bashkirtseva, A.B. Neiman, L. Ryashko, *Phys. Rev. E* **87**, 052711 (2013)
22. S. Patidar, A. Pototsky, N.B. Janson, *New J. Phys.* **11**, 073001 (2009)
23. D.V. Alexandrov, I.A. Bashkirtseva, A.P. Malygin, L.B. Ryashko, *Pure Appl. Geophys.* **170**, 2273 (2013)
24. D.A. Kessler, N.M. Shnerb, *New J. Phys.* **11**, 043017 (2009)
25. R.P. Denlinger, R.P. Hoblitt, *Geology* **27**, 459 (1999)

26. D. Dzurisin, J.W. Vallance, T.M. Gerlach, S.C. Moran, S.D. Malone, *Eos Trans. Am. Geophys. Union* **86**, 25 (2005)
27. C. Michaut, Y. Ricard, D. Bercovici, R.S.J. Sparks, *Nat. Geosci.* **6**, 856 (2013)
28. J.E. Kendrick, Y. Lavallée, T. Hirose, G. Di Toro, A.J. Hornby, S. De Angelis, D.B. Dingwell, *Nat. Geosci.* **7**, 438 (2014)
29. R.M. Iverson, D. Dzurisin, C.A. Gardner, T.M. Gerlach, R.G. LaHusen, M. Lisowski, J.J. Major, S.D. Malone, J.A. Messerich, S.C. Moran, J.S. Pallister, A.I. Qamar, S.P. Schilling, J.W. Vallance, *Nature* **444**, 439 (2006)
30. P.L. Moore, N.R. Iverson, R.M. Iverson, U.S. Geological Survey Professional Paper 1750 (2008)
31. R.S. Matoza, B.A. Chouet, *J. Geophys. Res. B* **115**, 12206 (2010)
32. D.V. Alexandrov, I.A. Bashkirtseva, L.B. Ryashko, *Nonlin. Processes Geophys.* **22**, 197 (2015)
33. P. Hänggi, H. Thomas, *Phys. Rep.* **88**, 207 (1982)
34. P.E. Kloeden, E. Platen, *Numerical Solutions of Stochastic Differential Equations* (Springer-Verlag, Berlin, 1999)
35. G.E.P. Box, M.E. Muller, *Ann. Math. Stat.* **29**, 610 (1958)